Sumatra Journal of Disaster, Geography and Geography Education: June, 2024. Vol.8. No.1. pp. 37-45
Disaster, Geography, Geography Education http://sjdgge.ppj.unp.ac.id/index.php/Sjdgge
ISSN : 2580 - 4030 (Print) 2580 - 1775 (Online), Indonesia

An Understanding of Volcanic Deposits With Two Dimensional Electrical Resistivity Imaging Survey at Talamau Mountain West Pasaman, Indonesia

*Dipo Caesario[1], Beni Aulia[1], Riko Maiyudi[2], Wahyu Budhi Khorniawan[3], Anita Galih Ringga Jayanti[3]

*[1]Department of Geography – Universitas Negeri Padang, Indonesia
[2]Department of Mining Engineering – Universitas Negeri Padang, Indonesia
[3]Department of Geological Engineering – Diponegoro University, Indonesia
Email: caesariodipo@fis.unp.ac.id

*Corresponding Author, Received: March 10, 2024. Revised: April 24, 2024. Accepted: June 02, 2024

ABSTRACT: Understanding the distribution and characteristics of volcanic deposits is crucial for assessing geological hazards and resource potential. This study employs a two-dimensional electrical resistivity imaging (2D ERI) survey to model the subsurface structure of volcanic deposits at Talamau Mountain in West Pasaman, Indonesia. The survey was conducted to map the spatial extent, depth, and composition of these deposits, providing insights into their geophysical properties. The 2D ERI technique, which measures the electrical resistance of subsurface materials, allowed for the differentiation between various types of volcanic deposits based on their resistivity contrasts. Results from the survey reveal distinct layers of volcanic breccia, coarse tuff, fine tuff, and lava flows which are segmented by a fault that runs northeast to southeast. It is apparent in the 3D modelling results of the inversion of three 2D cross-sectional profiles that the trend in volcaniclastic materials has changed from aggradation to progradation. The integration of 2D ERI data with 3D geological modelling and stratigraphic analysis enhances our understanding of the volcanic history and subsurface complexity of Talamau Mountain. This approach not only aids in volcanic hazard assessment but also contributes to the broader geophysical knowledge of volcanic terrains for geologists and hazard mitigation planners in Talamau volcanic regions.

Keywords: Talamau, Volcaniclastic, Resistivity Imaging, Volcanic Model

1. INTRODUCTION

The Talamau Mountain, located in West Sumatra, Indonesia, more precisely, is part of the West Pasaman district [1]. Talamau region is a geological treasure trove characterized by its diverse volcanic activity and associated sedimentary phenomena [2]. The Pasaman region is distinguished by a wide variety of geological formations. The Central Sumatra Fault Zone, which is a section of the broader Great Sumatran Fault (GSF) and comprises segments like Suliti, Sumpur, Barumun, Angkola, Siulak, Sianok, and Sumani, crosses this area [1]. The Permian–Cretaceous interval is responsible for the oldest rock formations, which are composed of intrusive and metamorphic rocks with varying degrees of metamorphism, from low-grade to high-grade, and ranging from diorite to granite [3], [4]. During the Eocene to Pliocene, sedimentary rocks (breccia, sandstone, and shale) as well as volcanic and pelagic materials were found in addition to volcanic rocks such as pyroclastic deposits and lava. One of the most prominent features of this area is its volcanic and volcaniclastic deposits from The Talamau, Malintang, and Sorikmarapi volcanoes, that produce which are fragments of volcanic material ejected during eruptions and subsequently deposited by various geological processes, such as alluvium and debris deposits. The quaternary volcanic rocks left over from the eruptions of the ancient Pasaman and Talamau volcanoes are among the youngest deposits recently exposed [4]. The products of the old Pasaman volcano consist of andesite-basaltic lava, volcanic lava, and volcaniclastics [3]. These deposits not only provide a historical record of volcanic activity but also offer insights into the dynamic interplay between tectonic movements, such as earthquakes, and surface processes like debris flows [1], [2], [3], [5].

The West Pasaman district was struck by an earthquake on Friday, February 25, 2022. With an epicentre on land at coordinates of 0.14° north latitude and 99.99° east longitude, the first foreshock happened at 08:35:51 WIB [2]. Apart from destroying more than 3312 houses and causing 10 deaths and more than 400 injuries, this

Sumatra Journal of Disaster, Geography and Geography Education: June, 2024. Vol.8. No.1. pp. 37-45
Disaster, Geography, Geography Education http://sjdgge.ppj.unp.ac.id/index.php/Sjdgge
ISSN : 2580 - 4030 (Print) 2580 - 1775 (Online), Indonesia

6.1 Mw earthquake also produced landslides (debris flows) along rivers and valleys around Mount Talamau [1], [2], [5]. The physical characteristics of both buried and superficial lithotypes, as well as the local geology, have a significant influence on the distribution of damage in affected areas. Subsoil heterogeneity does, in fact, cause changes in the amplitude and frequency of seismic waves as they travel through the uppermost geological layers [6]. Kajai village is one of the villages that was quite heavily affected by this earthquake and landslide disaster [1], [3], [4], [5], [7]. This is due to the fact that the Kajai Fault, one of the newly discovered faults that has never been mapped, is actively contributing to the earthquake's catastrophic effects in this region [3], [4]. Electrical Resistivity Imaging (ERI) is one of the tools that is quite widely used to map and analyze rock layers below the surface, starting from the survey, inversion and modelling stages [8], [9], [10], [11].

This ERI is based on Ohm's law, which is the fundamental principle of the resistivity method and estimates the potential on the earth's surface using the electrode potential and current flowing into the ground through the current electrode [10], [12]. The Wenner-Schlumberger configuration is one of the numerous configuration types that geoelectricity is built on [13]. It is suggested that this ERI is going to highlight the strong relationship between the subsurface conditions' geological, geomorphic, and geoelectrical parameters and their relevance to disaster vulnerability regions in this study area [11]. In this study, three 2D electrical resistivity imaging lines are proposed, named Line-1, Line-2, and Line-3, the distribution of which is depicted in Fig.1.

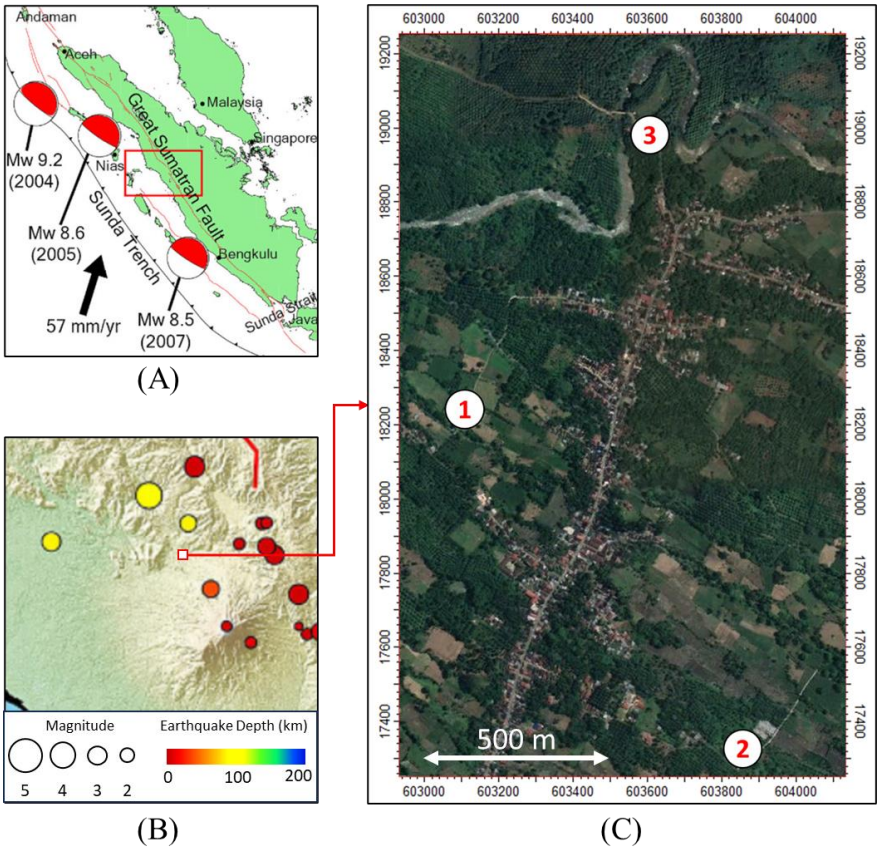

Fig 1. (A) West Pasaman is surrounded by the Great Sumatran Fault and active subduction tectonics.; (B) Distribution of the location of the epicentre, depth and magnitude of the earthquake near the study area.; (C) The distribution of 2D electrical resistivity imaging (ERI) measurement (Line-1, Line-2, and Line-3) locations in Kajai village.

2. METHODS

2.1 2D Resistivity Imaging

The current (I) and potential difference (ΔV) values for each position of the Schlumberger Werner setup are obtained using a resistivity meter of the Naniura brand. The Wenner Schlumberger

arrangement, also known as a lateral mapping depiction, is used in the geoelectrical approach to study variations in subsurface resistivity in a lateral (horizontal) direction [13]. Fig. 2 describes the Wenner configuration as a geoelectric technique that is typically limited to the earth's comparatively flat surface and uses equal spacing (a) between sounding locations (n) [12]. From each position of the electrode in the Wenner configuration, a resistivity value will be obtained which is calculated in the field as apparent resistivity (ρ_a) which will then be corrected with a geometric factor (K) to obtain a resistivity value (ρ) using formula (1) and (2) [14]. Then the 2D inversion will be carried out using ResIPy software [15]. From each stretch of the 2D profile measured at 3 points (FIg. 2), the range of resistivity values for each rock formation will then be interpreted according to field observations [16].

$$\rho_a = K \frac{\Delta V}{I} \quad \ldots\ldots (1)$$

$$K = 2\pi \left[\left\{\frac{1}{r_1} - \frac{1}{r_2}\right\} - \left\{\frac{1}{r_3} - \frac{1}{r_4}\right\}\right] \quad \ldots\ldots (2)$$

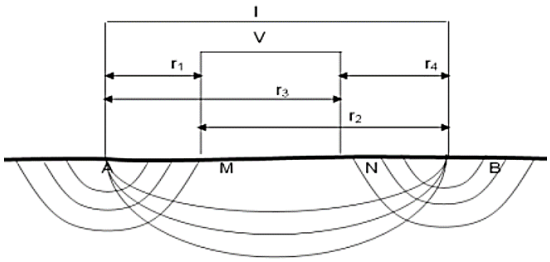

Fig 2. Wenner configuration with R_1=R_4=na and R_3=R_2=2na.

Transforming the apparent resistivity values into a genuine resistivity model of the subsurface is the aim of the inversion process. Before proceeding with forward modeling, an initial resistivity model is first built by utilizing the poisson equation to calculate the expected apparent resistivity value from the first model, which represents the distribution of the electric potential in the subsurface. Following that, a comparison is made between the measured and expected values, with the residual being kept below 3%.

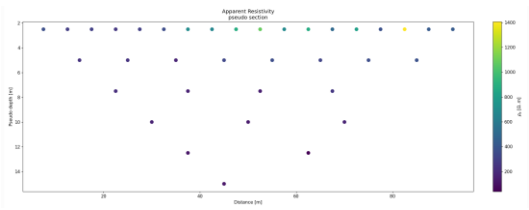

Fig 3. An example of apparent resistivity (Ohm.m) vs pseudo depth (m) in one Werner Schlumberger configuration before 2D inversion methods.

2.2 Volcanic Deposit Geomodeling

The technique of creating intricate, three-dimensional reconstructions of volcanic deposits and associated geological characteristics is known as "volcanic deposit geomodeling". Volcanic deposit geomodeling involves the integration of geological and geophysical data to build a 3D model of volcanic deposits [9]. These models are essential for various applications, including volcanic hazard assessment, resource exploration, and geological research. This proccess start with field observation and sample gathering to get a better comparison with the resistivity value.

3. RESULTS AND DISCUSSION

3.1 Petrology Of Volcanic Deposits

From observations on the surface of Line-1, Line 2, and Line 3, it is dominated by fresh volcanic deposits with coarse sand to gravel grain sizes which is depicted in Fig. 4.

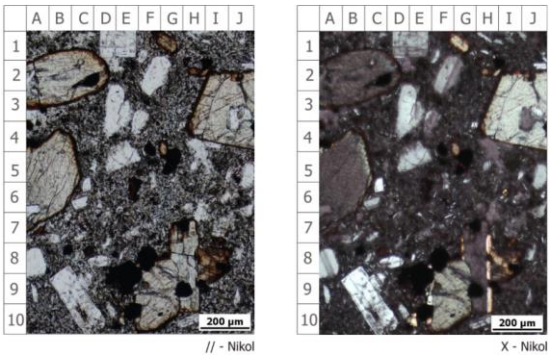

Fig 4. Petrography Thin Section on parallel dan cross nicol of fresh andesite lava fragments, which is dominated by the phenocrysts of the minerals Hornblenda (B5, B2, J3, and G9) and Plagioclase (C9, E1m and E3) on Line-1.

The volcanic rock andesite is characterized by its distinct porphyritic texture, which features prominent phenocrysts—crystals that are significantly larger than the surrounding groundmass—measuring up to 2.0 mm in size. These phenocrysts include minerals such as pyroxene, hornblende, and various opaque minerals, all embedded within a very fine-grained matrix. This groundmass is primarily composed of plagioclase cryptolite, along with secondary minerals such as iron oxide and clay. Additionally, the andesite rocks display vesicles, which are small cavities that formed due to the presence of gas bubbles during the solidification of the lava.

Phenocrysts make up about 35-40% of the overall rock composition. Plagioclase appears as one of the primary phenocrysts, exhibiting polysynthetic twinning and compositional zoning. These plagioclase crystals are often altered to secondary clay minerals and feldspars over time. The mafic minerals present in the andesite, predominantly pyroxenes with some hornblende, also appear as phenocrysts. These mafic phenocrysts frequently show signs of alteration, such as coatings of iron oxide. Black opaque minerals are observed both as standalone phenocrysts and as inclusions within the plagioclase, pyroxene, and hornblende phenocrysts.The groundmass of andesite is an intricate mixture of plagioclase cryptolite, iron oxide, and clay minerals. In addition to the mineral composition, the orientation of the plagioclase microliths and other mineral components within the groundmass reveals a flow texture, particularly noticeable along Line-2. This flow texture is indicative of the dynamic processes that occurred during the rock's formation, reflecting the movement and cooling of the molten material from which the andesite solidified.

Table 1. The geological units are identified using the electrical resistivity range [3].

No	Code of Color	Geological Unit	Resistivity (Ohm.m)	
			Min	Max
1	Red	Lava Andesite (Fragment)	>1000	
2	Dark Brown	Volcanic Breccia (Matrix)	320	1000
3	Light Brown	Coarse Tuff	80	320
4	Green	Fine Tuff	2	80

Source: Results of data analysis, 2022.

3.2 Electrical Resisitivity Imaging

This study obtained a spread of resistivity values between 2 ohms and 2000 ohms from the inversion results on 3 corrected lines. These values were then grouped based on observations of lithology on the surface that had been examined in petrography in the previous step. The rock lithology units were divided into 4 groups according to their resistivity values, which were then summarized in Table 1.

On line-1 a 100m distance of spans measurement are obtained and showing a lower resitivity value which is interpreted as fine tuff and coarse tuff deposits. slightly different from Line-2 and line-3 which are characterized by the appearance of high resistivity values of up to more than 1000 ohm.m which are interpreted as andesite lava fragments embedded in the breccia matrix, It is displayed on the map in Figure 5 below.

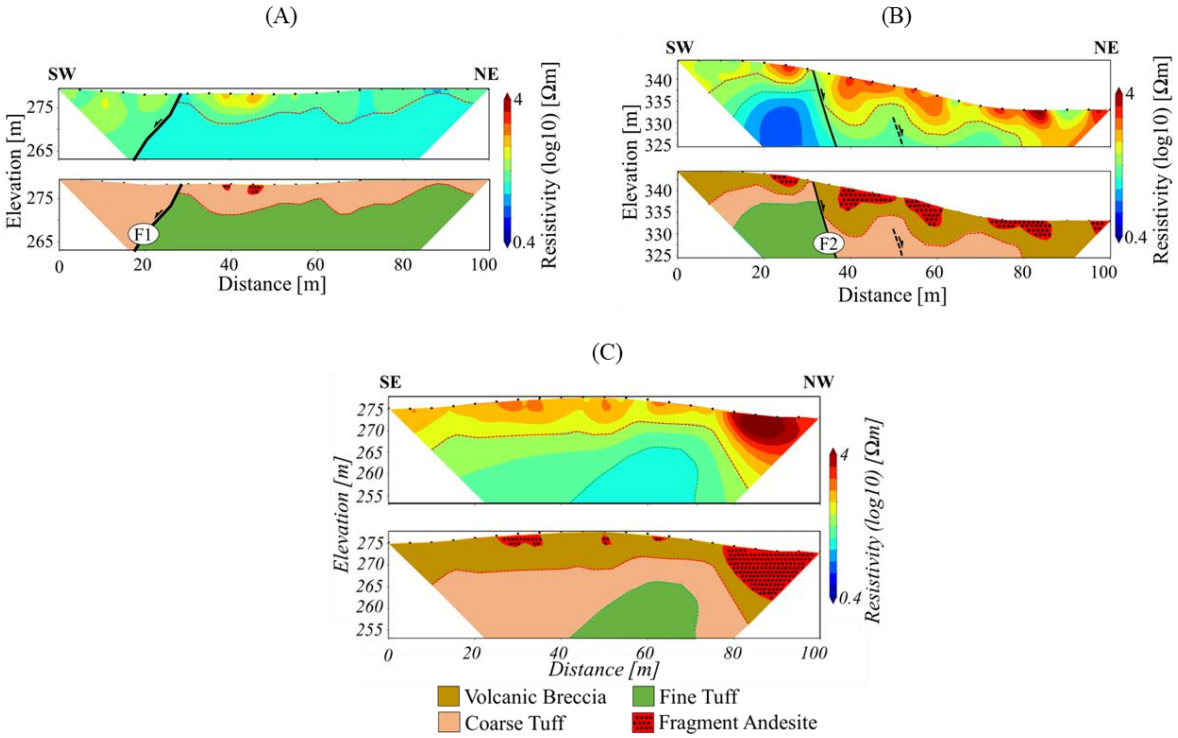

Fig.5 The interpertation of lateral and vertical Resisitvity value and lithology unit distribution from Line-1 (A), Line-2 (B), and Line-3 (C).

3.3 3D Volcanic Deposit Model

A 3D Volcanic Deposit Model was constructed using geostatistical methods, leveraging three pre-built cross-sections as seen in Fig 6. Topography and fault surfaces were used as key inputs for the model. The initial step in the 3D modeling process involved creating a grid model with surface topographic limits extending up to 240 meters above sea level. Subsequently, a directional cell grid with dimensions of 5m x 5m x 0.5m was generated. This grid was based on the kriging results of the boundary height map between fine tuff (green) and coarse tuff (light brown), which were derived from the height points of the three 2D electrical resistivity imaging lines.

To refine the model, resistivity measurements from the three datasets were upscaled, followed by geostatistical analysis to produce an analytical variogram oriented towards the caldera mouth of Mount Talamau (N285ºE). The sequential Gaussian simulation method was employed to distribute the resistivity values within the grid, with weighting influenced by the distance to the Talamau caldera mouth.

The resulting 3D model reveals the occurrence of at least two volcaniclastic deposit events, identified as progradation and aggradation events, separated by an eruption boundary. The youngest deposits show significant variation in thickness, with the average thickness ranging from 13.2 meters to a maximum of 43.8 meters in the thickest areas. This detailed modeling provides valuable insights into the volcanic deposit patterns and the geological history of the area surrounding Mount Talamau..

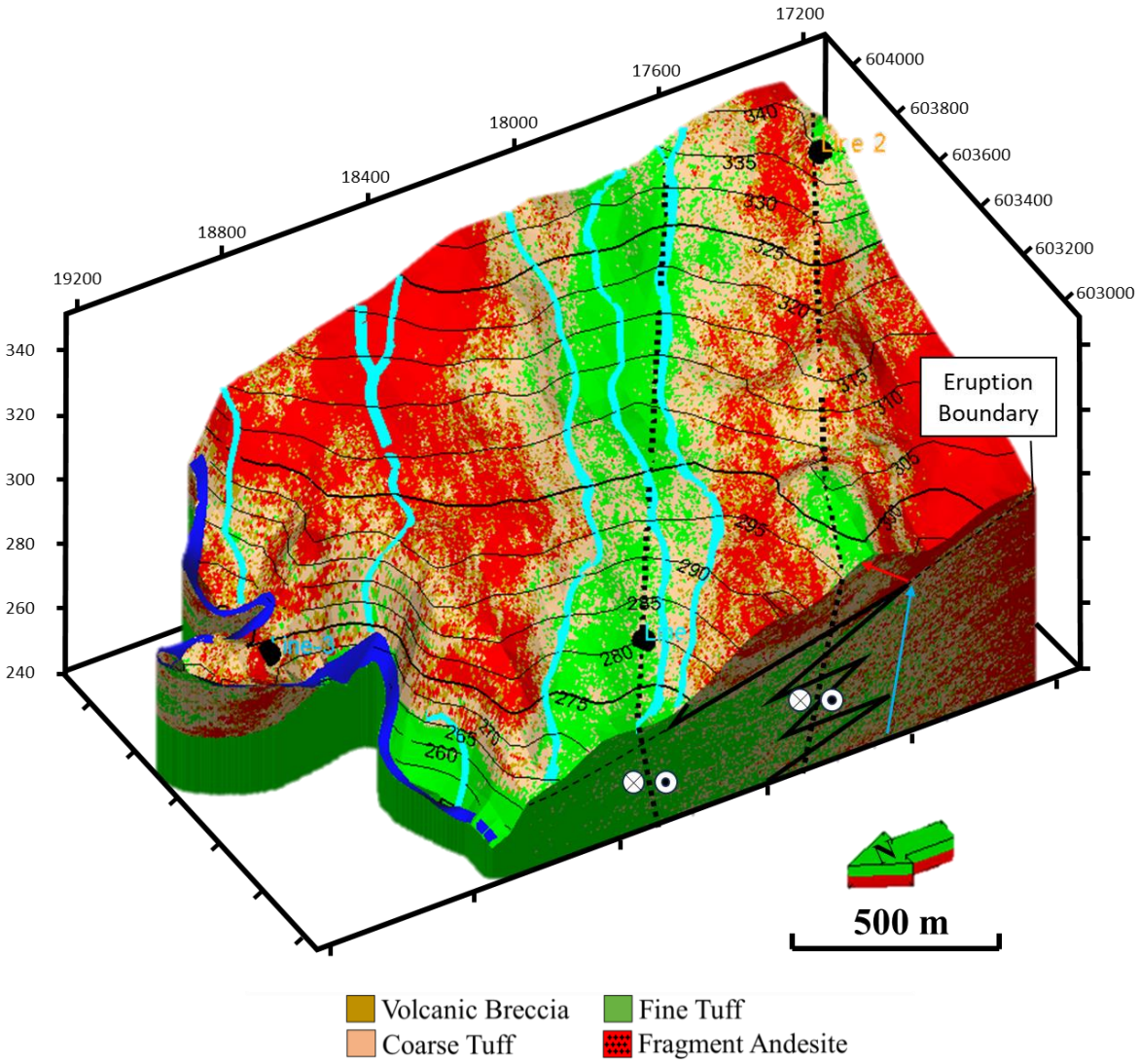

Fig. 6. 3D Model of volcanic deposit provides valuable insights into the geological and resistivity characteristics of the Kajai Village and surroundings highlighting areas of varying resistivity, structural features, and progradation (red arrow) and aggradation (blue arrow) volcaniclastic event.

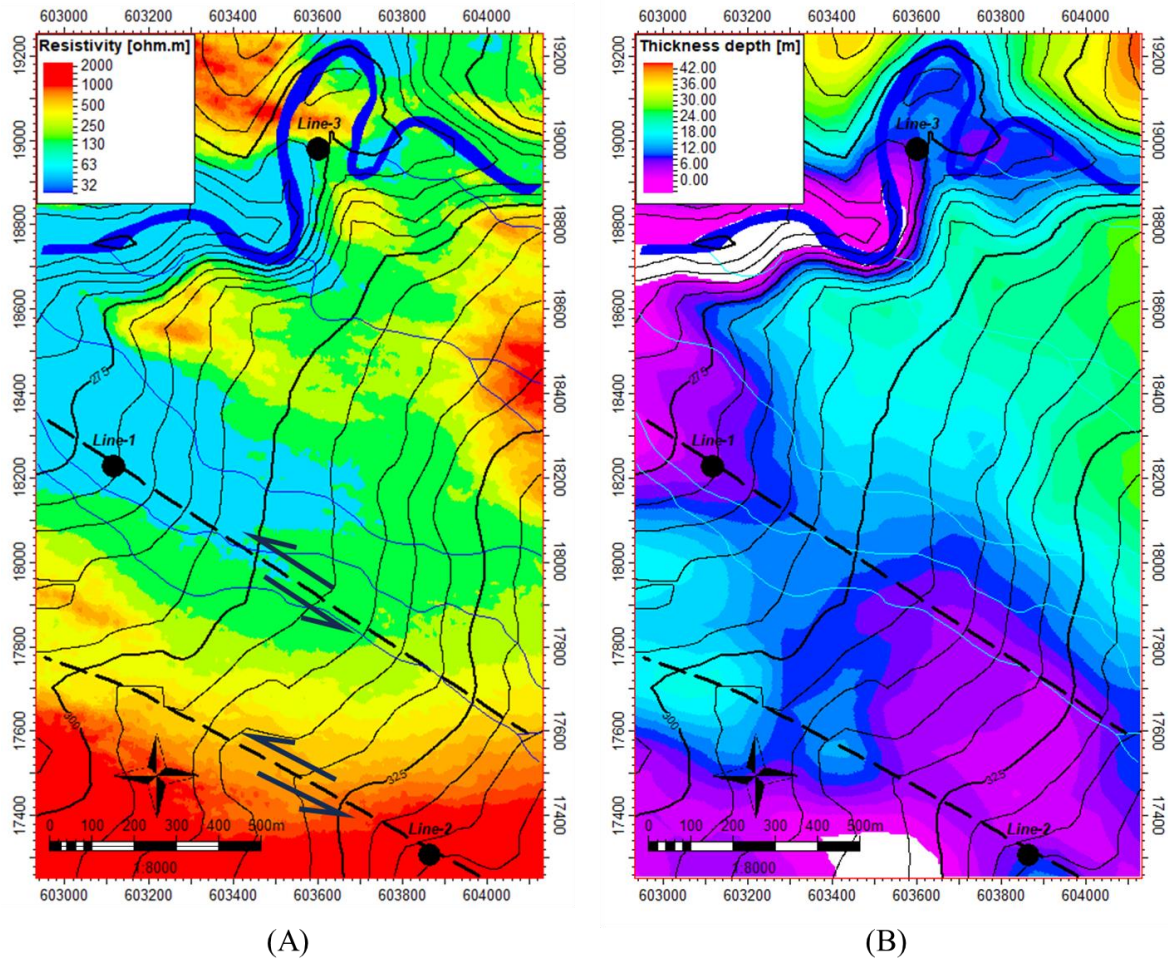

Fig. 7 (A).The average resistivity map, which displays values from topography to 240 meters above sea level, reveals a significant contrast in values in the area near to the Kajai strike-slip fault.; and (B). thickness map of the youngest volcaniclastic deposits showing thinning in the area closest to the Kajai strike slip fault.

An average thickness map and an average resistivity value map were generated from the 3D volcanic deposit model, both of which are shown in Fig. 7. This suggests that the Kajai strike slip fault was active during this period while the last of the volcaniclastic deposits were deposited since it indicates the thinning of volcaniclastic deposits alongside with the fault's active activity.

4. CONCLUSION

Kajai village and its surroundings are situated in areas characterized by low resistivity values, typically less than 50 ohm.m, which indicate the presence of fine tuff deposits. These deposits have excellent porosity, making them beneficial for groundwater aquifers, which can be an important resource for the local population. However, the same geological characteristics that make the tuff deposits good for aquifers also pose significant risks.

One major risk is the amplification of earthquake vibrations. If the Kajai fault, which is known to be active, were to become reactivated, the fine tuff deposits could intensify seismic waves, leading to stronger ground shaking. This amplifying effect increases the earthquake hazard in the region, making it a high-potential area for seismic activity.

Additionally, the region's geological setting poses a risk for volcanic debris flows, especially during heavy rainfall or volcanic eruptions. The graben areas, which are low-lying zones formed by the active faulting of the Kajai fault south of the village, can funnel and accelerate debris flows. These flows are further exacerbated by the presence of large deposits of andesite fragments and volcanic breccia along the Batang Tonggar River. These materials can be easily mobilized by water, leading to potentially destructive debris flows that can impact the village and its surroundings.

In summary, while the fine tuff deposits provide essential aquifer resources, they also contribute to the area's vulnerability to earthquakes and debris flows. This duality underscores the need for careful land use planning and disaster preparedness measures in Kajai village to mitigate these natural hazards.

5. ACKNOWLEDGEMENTS

Thanks to the assistance and collaboration of numerous parties, this research can be completed without incident. Thus, the Institute for Research and Community Service (LPPM) of Universitas Negeri Padang is thanked by the author for providing research funds under the Rector's Decree Number 238/UN.35/LT/2022. They have given us the chance and the time to hone our academic skills, particularly in the area of volcanic disasters. The Center for Spatial Data Infrastructure Development Studies (PPIDS UNP), Nada Fauziah, M. Raihan Al Faruq, Pebriadi Pratama, Galang Ridho, and the Kajai Sub-district regional administration were also acknowledged to the fullest amount.

6. REFERENCES

[1] B. G. Dewanto *et al.*, “The 2022 Mw 6.1 Pasaman Barat, Indonesia Earthquake, Confirmed the Existence of the Talamau Segment Fault Based on Teleseismic and Satellite Gravity Data,” *Quaternary*, vol. 5, no. 4, p. 45, Nov. 2022, doi: 10.3390/quat5040045.

[2] F. Bari, B. Istijono, R. Yuhendra, A. Hakam, M. Noer, and T. Ophiyandri, “Potential debris flow after earthquake in Mount Talamau Pasaman district and West Pasaman district,” *IOP Conf. Ser.: Earth Environ. Sci.*, vol. 1173, no. 1, p. 012069, May 2023, doi: 10.1088/1755-1315/1173/1/012069.

[3] Y. Suasti, D. Caesario, W. J. Prihantarto, B. B. Susetyo, and P. Iskarni, “DEVELOPMENT OF ACTIVE FAULT MAPPING METHOD USING GEOELECTRIC AND GEOGRAPHICAL INFORMATION SYSTEM,” *GEOMATE*, vol. 26, no. 116, Apr. 2024, doi: 10.21660/2024.116.4360.

[4] P. Supendi *et al.*, “A previously unidentified fault revealed by the February 25, 2022 (Mw 6.1) Pasaman Earthquake, West Sumatra, Indonesia,” *Physics of the Earth and Planetary Interiors*, vol. 334, p. 106973, Jan. 2023, doi: 10.1016/j.pepi.2022.106973.

[5] R. F. Zakir, A. Hakam, B. Istijono, M. Noer, and S. Rahmadilla Hape, “Vulnerability Assessment of non-engineered houses related to earthquake in West Pasaman District,” *IOP Conf. Ser.: Earth Environ. Sci.*, vol. 1173, no. 1, p. 012075, May 2023, doi: 10.1088/1755-1315/1173/1/012075.

[6] M. Moscatelli *et al.*, “Physical stratigraphy and geotechnical properties controlling the local seismic response in explosive volcanic settings: the Stracciacappa maar (central Italy),” *Bull Eng Geol Environ*, vol. 80, no. 1, pp. 179–199, Jan. 2021, doi: 10.1007/s10064-020-01925-5.

[7] N. Fauziah and A. Yulfa, “Microzonation mapping of building damage after earthquake disaster in Nagari Kajai West Pasaman district,” in *Eighth Geoinformation Science Symposium 2023: Geoinformation Science for Sustainable Planet*, SPIE, Jan. 2024, pp. 411–423. doi: 10.1117/12.3009712.

[8] R. M. Antosia, Mustika, I. A. Putri, S. Rasimeng, and Dinata, “Andesite prospect at West Sungkai of North Lampung: Its distribution based on electrical resistivity tomography,” *IOP Conference Series: Earth and Environmental Science*, vol. 882, no. 1. 2021. doi: 10.1088/1755-1315/882/1/012086.

[9] A. Platz *et al.*, “3D imaging of the subsurface electrical resistivity structure in West Bohemia/Upper Palatinate covering mofettes and Quaternary volcanic structures by using Magnetotellurics,” *Tectonophysics*, vol. 833. 2022. doi: 10.1016/j.tecto.2022.229353.

[10] D. Parwatiningtyas, R. Y. Astuti, and P. Hartoyo, “Application of 2D resistivity from geoelectrical methods with dipole dipole configuration for identification of land slides in Citeko Village, Cisarua, Bogor District, West Java,” *Journal of Physics: Conference Series*, vol. 1832, no. 1. 2021. doi: 10.1088/1742-6596/1832/1/012015.

[11] G. Gupta *et al.*, “Electrical resistivity imaging for aquifer mapping over Chikotra basin, Kolhapur district, Maharashtra,” *Environ Earth Sci*, vol. 73, no. 12, pp. 8125–8143, Jun. 2015, doi: 10.1007/s12665-014-3971-5.

[12] N. Dengen, “PENGOLAHAN DATA GEOLISTRIK PADA EKPLORASI SUMBER AIR TANAH DI KECAMATAN KONGBENG KABUPATEN KUTAI TIMUR DENGAN PERANGKAT LUNAK RES2DINV,” *Jurnal Informatika Mulawarman*, vol. 7, no. 1, pp. 27–34, Feb. 2012.

[13] D. Chandrasasi, R. Asmaranto, Jurusan Teknik Pengairan, Fakultas Teknik, Universitas Brawijaya, Malang, N. M. C. Partarini, and Jurusan Teknik Pengairan, Fakultas Teknik, Universitas Brawijaya, Malang, “PENERAPAN METODE GEOLISTRIK KONFIGURASI WENNER –

SCHLUMBERGER UNTUK ANALISIS REMBESAN PADA MAINDAM WADUK GRENENG, KABUPATEN BLORA," *pengairan*, vol. 9, no. 2, pp. 114–124, Nov. 2018, doi: 10.21776/ub.pengairan.2018.009.02.5.

[14] M. Marwan *et al.*, "Geoelectrical model of geothermal spring in Ie Jue Seulawah deriving from 2D VLF-EM and DC resistivity methods," *J Appl Eng Science*, vol. 21, no. 2, pp. 59–69, 2023, doi: 10.5937/jaes0-38014.

[15] G. Blanchy, S. Saneiyan, J. Boyd, P. McLachlan, and A. Binley, "ResIPy, an intuitive open source software for complex geoelectrical inversion/modeling," *Computers & Geosciences*, vol. 137, p. 104423, Apr. 2020, doi: 10.1016/j.cageo.2020.104423.

[16] F. Alshehri and K. Abdelrahman, "Groundwater resources exploration of Harrat Khaybar area, northwest Saudi Arabia, using electrical resistivity tomography," *Journal of King Saud University - Science*, vol. 33, no. 5, p. 101468, Jul. 2021, doi: 10.1016/j.jksus.2021.101468.